Using Laser in the Fabrication of Graphene for Gas Sensing: A Digital Twin Approach

José Carlos Santos-Ceballos[1], Foad Salehnia[*1], Alfonso Romero[1], and Xavier Vilanova[1]

[1]*Universitat Rovira i Virgili, Microsystems Nanotechnologies for Chemical Analysis (MINOS), Tarragona, Spain*
[*]*Corresponding author's e-mail: foad.salehnia@urv.cat*

Laser-induced graphene (LIG) is a novel 3D porous material formed by laser treatment of specific carbon substrates, boasting remarkable properties including high porosity, electrical conductivity, and mechanical flexibility. Understanding the relationship between laser parameters and resulting LIG characteristics is fundamental, and often investigated through computational methods. Leveraging its unique attributes, LIG finds application in sensors, particularly gas sensing, owing to its characteristics and facile fabrication process. This study employs a digital twin to predict LIG characteristics and explore their correlation with nitrogen dioxide (NO_2) gas sensing efficacy. LIG sensors with various morphologies (woolly fibers, porous formation, cellular network) and electrical resistances were fabricated and assessed for response and recovery to NO_2 exposure. Results demonstrate morphology-dependent performance, with woolly fibers morphology showing optimal response and recovery at low resistance values. Conversely, porous formations and cellular networks exhibit superior response at high resistance values but complete recovery at lower values. These findings underscore the critical role of laser parameter optimization in tailoring LIG for enhanced gas sensing capabilities.
DOI: 10.2961/jlmn.2024.02.2005
Keywords: digital twin, laser-induced graphene, gas sensing, machine learning, sensors

1. Introduction

Laser-induced graphene (LIG) is a newly emerging 3D porous material crafted through the precise application of a laser beam on certain carbon precursor materials (e.g., polymers, leaf, paper, wood, and food) [1–4]. This single-step method has surfaced as a substitute for conventional approaches to obtaining graphene. It can be performed in ambient air without any solvents, wet chemical procedures, subsequent treatments, or other supporting processes making it exceedingly attractive for industrial use [5-6].

The unique properties of LIG, including high porosity, mechanical flexibility, and outstanding electrical conductivity, position it as an ideal material for a wide range of applications. These range from energy storage devices as supercapacitors [7], batteries [8]) and triboelectric nanogenerators [9], to microfluidic systems [10], catalysis systems [11], and water purification [12]. Additionally, LIG has been used in sensor applications including biosensors [13], and physical sensors [14-15]. Particularly noteworthy is its use in gas sensing due to its sensitivity and selectivity [16–21].

The optimization of laser graphitization involves tailoring process parameters, like average laser power and scan speed, to specific materials. These parameters enable the direct writing of 3D porous structures with graphene-like carbon. Avoiding nonoptimal laser settings is crucial to prevent undesired effects such as material ablation or incomplete graphitization [1-22]. The intricate relationship between the laser configuration parameters and the LIG characteristics obtained has been extensively studied, and several researchers have used computational methods to understand this relationship [23-24].

Digital twins are becoming increasingly important, offering virtual representations of physical machines, complicated processes, and complex systems through computational models. In material science and chemical synthesis, digital twins accelerate the development of new materials by depicting their structure, processes, and performance evolution [25]. They enable predictions of material behavior under different conditions and optimize manufacturing processes to ensure materials meet the required specifications [26]. In the case of the LIG, laser parameters have been virtually tested to understand their relationship with the syntheses through simulations within the digital twin [27]. This has helped to predict the characteristics of the material without physically experimenting, saving time and resources.

This work used a digital twin previously developed by our research group to estimate the characteristics of the fabricated LIG layer (morphology, electrical resistance) [27]. This simulation, integrated with machine learning techniques, explored the interplay between LIG's characteristics and its efficacy in nitrogen dioxide (NO_2) gas sensing.

2. Materials and methods

2.1 Sensing device fabrication and gas-sensing measurements

To understand the influence of the characteristics of the LIG layer for gas detection, the workflow depicted in the diagram in Fig. 1 has been followed. The digital twin was initially employed to predict LIG's characteristics by various laser parameters (speed, frequency, and power).

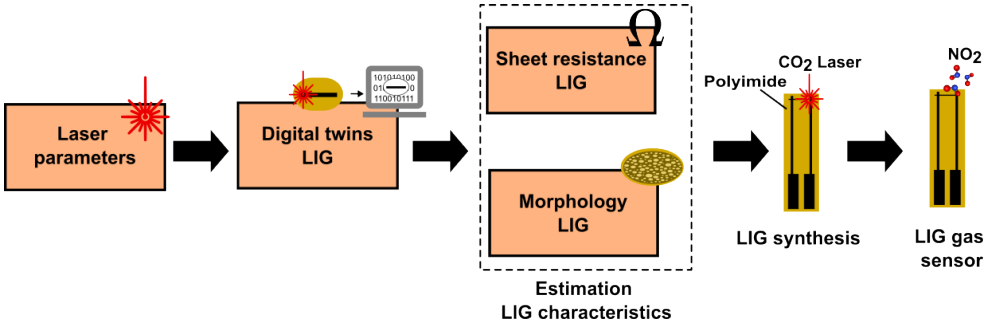

Fig. 1 Block diagram shows the workflow in this research.

The models used were obtained through machine learning algorithms, specifically utilizing artificial neural networks and Gaussian process regression. This approach generated samples with three distinct morphologies (woolly fibers (WF), cellular networks (CN), and porous formations (PF)) exposed by Abdul Hafez et al. [22]. Each type exhibited different electrical resistance values. Table 1 shows the different combinations of laser parameters (speed, frequency, and power) used and the results obtained. Subsequently, various gas sensors were fabricated. The LIG gas sensors were fabricated using a commercial polyimide film (50 µm thickness) as the substrate. LIG was synthesized using a carbon dioxide (CO_2) laser system (SYNRARD 48-2) with a wavelength of 10.6 µm and a maximum power of 25 W. The gas sensors feature a sensitive area comprising a straight line LIG (6 mm long and a width equal to 116 µm), with the previously predicted characteristics.

Then, the gas-sensing performance of manufactured sensors was evaluated in the gas measurement system shown in Fig. 2. The sensors were put in an airtight Teflon chamber with a volume of 35 cm^3 at room temperature. The detection chamber was connected to a gas supply and mixing system that used a cylinder of 100 ppm NO_2 and another cylinder of pure, dry air as a carrier. Then, the resistance of the different sensors was monitored using a multimeter (HP 34972A, Agilent), and resistance changes were recorded while 50 ppm of NO_2 was applied. The sensors were stabilized under dry air for 120 minutes before exposure to NO_2 species for 15 minutes. To work under more realistic experimental conditions, the total flow was adjusted at a low rate (100 mL/minute) using a set of mass-flow controllers (Bronkhorst High-Tech B.V.) and electro valves. The sensor response is defined as $\Delta R/R_0$ expressed in percentage, where ΔR corresponds to the resistance changes recorded over gas exposure (15 minutes), while R_0 is given by the sensor's resistance in the air (or baseline); simultaneously evaluating sensitivity and response time. Also, sensor recovery (the percentage of resistance recovery to the baseline 60 minutes after gas exposure) was analyzed.

Table 1 Shows the laser parameters (power, speed, frequency) used, the LIG characteristics (morphology, electrical resistance) obtained and the gas sensing performance (response, recovery) of each of the sensors.

Power (%)	Speed (mm/s)	Frequency (kHz)	Morphology	R_0 (kΩ)	$\Delta R/R_0$ (%)	Recovery (%)
50	400	5	WF	15.1	0.8	100.0
50	500	15	WF	16.5	1.0	100.0
40	700	17.5	WF	26.1	0.4	90.5
50	800	10	WF	35.7	0.9	75.6
20	300	17.5	PF	11.9	0.6	100.0
10	300	15	PF	20.2	0.6	82.3
30	600	15	PF	25.4	0.8	68.4
30	700	20	PF	29.7	0.9	70.1
5	75	15	CN	10.9	0.8	100.0
10	200	7.5	CN	20.2	0.6	85.9
30	600	20	CN	28.1	1.1	61.6
30	500	10	CN	32.7	1.2	78.1

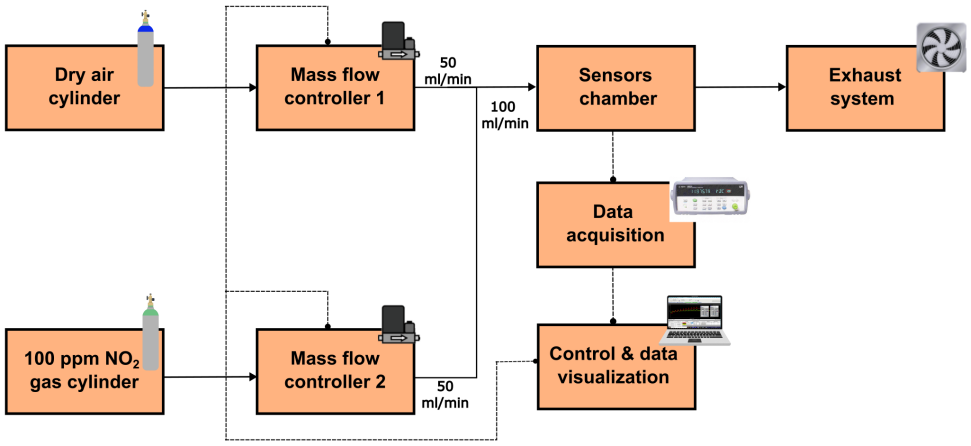

Fig. 2 Block diagram shows the gas measurement system.

2.2 Characterization of the gas-sensitive materials

A Scios 2 DualBeam field emission scanning electron microscope (FESEM) was used to analyze the morphology of the synthesized layers. The Raman analysis was conducted using a Raman spectrometer (Renishaw plc) with a coupled confocal Leica DM2500 microscope (Leica Microsystems GmbH) with a laser of 514 nm wavelength.

3. Results and discussion

3.1 Structural and morphological studies of LIG

The FESEM images (Fig 3) from the fabricated LIG gas sensor samples depict the three morphologies cited previously. Fig. 3a shows the initial stages of carbonization (porous formation), marked by the formation of porosity, wherein the polyimide precursor undergoes a transformative process, yielding graphene-like structures. The formation of interconnected cellular networks of 3D graphene is shown in Fig. 3b. The presence of this morphology underscores the unique structural properties of the fabricated material, which are distinct from conventional two-dimensional graphene structures. In contrast, a remarkable transition to a fibrous morphology characterized by the presence of woolly fibers was observed under conditions of high laser fluxes. This observation suggests that the laser flux plays a pivotal role in dictating the final morphology of the fabricated material, influencing the spatial arrangement and structural characteristics of the LIG.

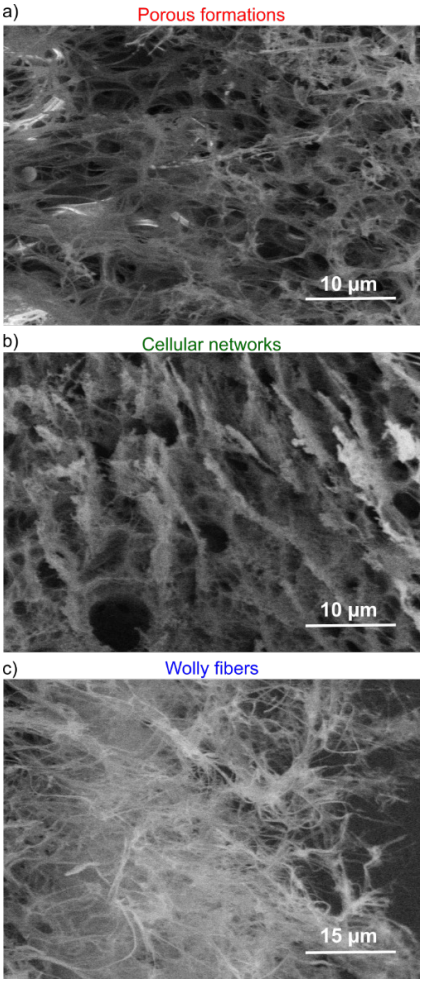

Fig. 3 Field emission scanning electron microscope (FESEM) images of a) porous formations, b) cellular networks and c) woolly fibers morphologies.

Raman spectroscopy was performed along the LIG layers to investigate the correlation between the morphologies and molecular structure of LIG. In the Raman spectrum (Fig.4) corresponding to the PF morphology, the appearance of G and D peaks is observed, located in the typical positions (around 1580 cm^{-1} and 1350 cm^{-1}) of the graphite formation in the material [6-22-23-28]. Furthermore, peaks G and D show a large full width at half maximum (FWHM), which covers a wide band around the 2D peak, indicating the presence of porous graphite structures. The CN morphology exhibits a distinctive spectral signature characterized by a sharper and more well-defined 2D band, accompanied by a notable reduction in the FWHM of both the G and D peaks. The reduction in FWHM of the G peak suggests the formation of larger sp^2 grains within the material, indicating the development of 3D graphene structure. The WF morphology showed similar Raman spectra to those of the PF, characterized by the absence of a sharp 2D peak and a larger FWHM for the G peak compared to the cellular networks. These results suggested that woolly fibrous structures possess lower-quality sp^2 carbon than network cellular structures.

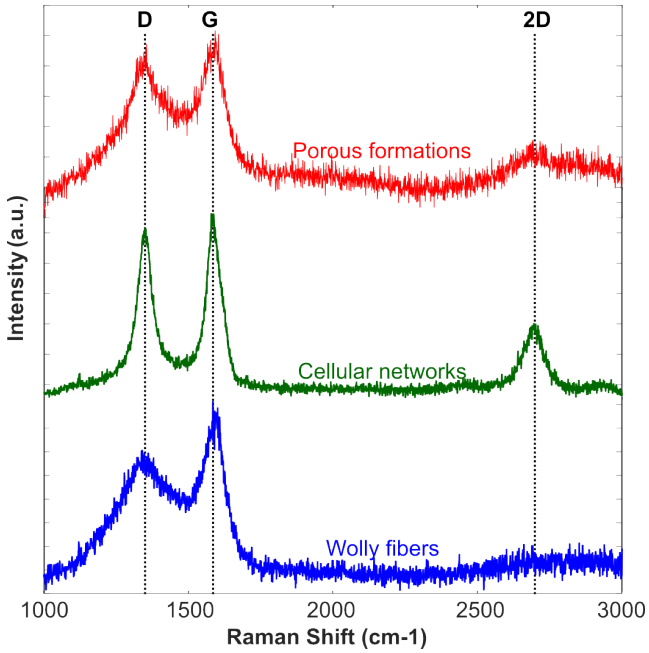

Fig. 4 Raman spectra of porous formations (red line), cellular networks (green line) and woolly fibers (blue line) morphologies.

3.2 Gas sensing performance of LIG

The sensing performance of the LIG gas sensors developed for NO_2 detection was assessed under conditions like those required for real-time monitoring. Fig. 5 illustrates the electrical response observed for one of the LIG gas sensors fabricated, which exhibited decreased resistance upon exposure to the target gas (50 ppm of NO_2). The reduced resistance results from the increased hole density and electrical conductivity of the p-type LIG upon exposure to the oxidating NO_2 species. Additionally, it is observed that the sensor can increase its electrical resistance until it recovers the baseline when it stops being exposed to NO_2. The longer recovery time (60 minutes) compared to the response time (15 minutes), is attributed to the persistence of gas molecules within the sensitive layer, requiring a longer duration for

desorption or complete elimination during re-exposure to air. Considering that this experiment has been carried out at room temperature, the use of a heater or ultraviolet light would facilitate the desorption of the gas, thus reducing the recovery time [29–31].

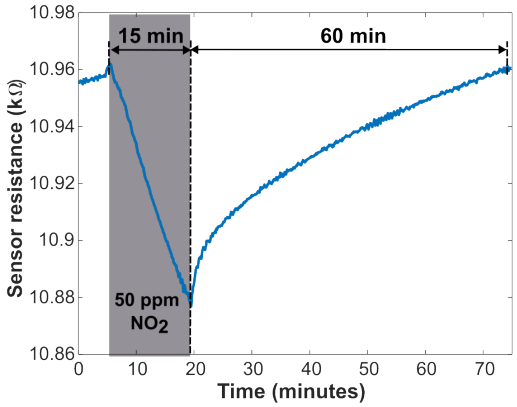

Fig. 5 Electrical response of a LIG gas sensor under 50 ppm of NO_2.

Fig. 6(a and b) reveals that, in the case of the first phase of graphitization (PF morphology), the response of the sensors is better at high electrical resistance baseline values (R_0). However, at low values, the sensor recovery is complete (100% in less than 50 minutes). This performance pattern is also observed in samples with CN morphology (Fig. 6(c and d)). The WF morphology (Fig. 6(e and f)) exhibits improved response and recovery at low electrical resistance values. Conclusively, an intelligent selection of the laser's parameters in the fabrication of LIG is crucial for optimizing their gas sensing capabilities. The study establishes that LIG with a woolly fibers morphology and low electrical resistance exhibits the most promising characteristics for effective gas sensing applications.

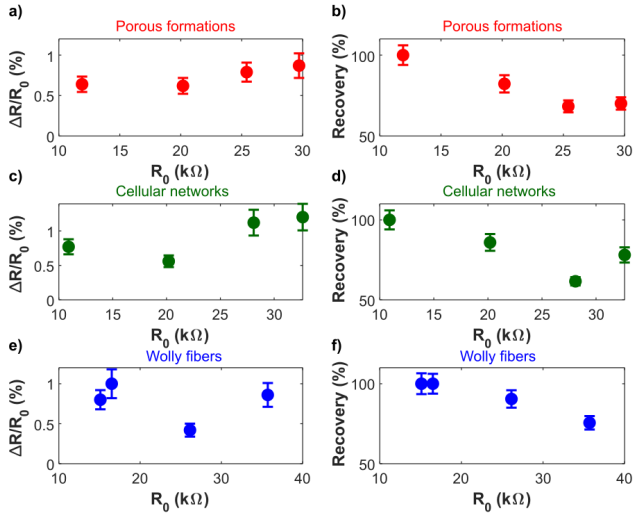

Fig.6 Sensors response (left side) and sensor recovery (left side) corresponding to LIG gas sensors with different morphologies and baseline electrical resistance.

4. Conclusions

In conclusion, laser-induced graphene (LIG) stands out as a versatile material with exceptional properties for gas sensing applications. Through meticulous control of laser parameters, LIG can be precisely tailored to exhibit specific morphologies and electrical resistances, influencing its performance in detecting gases such as NO_2. Our study, integrating digital twin simulations and machine learning techniques, highlights the importance of this parameter optimization process. We observed that LIG with woolly fibers morphology and low electrical resistance shows the most promising characteristics for effective gas sensing. However, we also noted that different morphologies exhibit distinct response and recovery patterns, indicating a nuanced relationship between morphology, resistance, and sensing performance. These findings underscore the significance of intelligent material design in maximizing gas sensing capabilities. Moving forward, further exploration into the underlying mechanisms governing the relationship between LIG characteristics and gas sensing performance will be crucial for advancing the development of highly efficient and selective gas sensing technologies. Considering the results of this work, our next investigations will be directed in two main directions. The first involves using the same methodology to explore the relationship between the characteristics of the LIG in different sensing areas with digital twins and the second is improving the gas sensing performance of the LIG by doping and compositing it with other materials, such as metal oxides or metals for selective gas sensors.

Acknowledgments

The research has been funded by the EU in the framework of Marie Sklodowska-Curie Actions, grant 823895-PE; MICINN, grants PDC2022-133967-I00 and TED2021131442B-C31, as well as AGAUR grant 2021 SGR 00147, J.C.S-C. Thanks to the predoctoral program AGAUR-FI ajuts (2023 FI-2 00180) Joan Oró of the Secretariat of Universities and Research of the Department of Research and Universities of the Generalitat of Catalonia and the European Social Plus Fund, F.S. thanks the Spanish Ministry of Universities, Recovery, Transformation, and Resilience Plan, and the Maria Zambrano grant Funded by the European Union – NextGenerationEU (grant number 2021URV-MZ-13).

References

[1] T. D. Le, H. Phan, S. Kwon, S. Park, Y. Jung, J. Min, B. J. Chun, H. Yoon, S. H. Ko, S. Kim, and Y. Kim: Adv. Funct. Mater., 32, (2022) 2205158.
[2] R. Ye, D. K. James, and J. M. Tour: Adv. Mater., 31, (2019) 1803621.
[3] Y. Chyan, R. Ye, Y. Li, S. P. Singh, C. J. Arnusch, and J. M. Tour: ACS Nano., 12, (2018) 2176.
[4] J. Lin, Z. Peng, Y. Liu, F. Ruiz-Zepeda, R. Ye, E. L. G. Samuel, M. J. Yacaman, B. I. Yakobson, and J. M. Tour: Nat. Commun., 5, (2014) 5714.
[5] K. Avinash, and F. Patolsky: Mater. Today., 70, (2023) 104.
[6] R. Ye, D. K. James, and J. M. Tour: Acc. Chem. Res., 51, (2018) 1609.
[7] W. Ma, J. Zhu, Z. Wang, W. Song, and G. Cao: Mater. Today Energy., 18, (2020) 100569.
[8] F. Zhang, E. Alhajji, Y. Lei, N. Kurra, and H. N. Alshareef: Adv. Energy Mater., 8, (2018) 1800353.
[9] K.-H. Choi, S. Park, S.-K. Hyeong, S. Bae, J.-M. Hong, T.-W. Kim, S. H. Lee, S. Ryu, and S.-K. Lee: J. Mater. Chem. A, 8, (2020) 19822.

[10] J. Zhu, X. Huang, and W. Song: ACS Nano., 15, (2021) 18708.
[11] X. Han, R. Ye, Y. Chyan, T. Wang, C. Zhang, L. Shi, T. Zhang, Y. Zhao, and J. M. Tour: ACS Appl. Nano Mater., 1, (2018) 5053.
[12] N. H. Barbhuiya, A. Kumar, and S. P. Singh: Trans. Indian Natl. Acad. Eng., 6, (2021) 159.
[13] Z. Wan, N.-T. Nguyen, Y. Gao, and Q. Li: Sustainable Mater.Technol., 25, (2020) e00205.
[14] A. Kaidarova, and J. Kosel: IEEE Sens. J., 21, (2021) 12426.
[15] S. Movaghgharnezhad, and P. Kang: J. Mater. Chem. C., 12, (2024) 6718.
[16] M. G. Stanford, K. Yang, Y. Chyan, C. Kittrell, and J. M. Tour: ACS Nano., 13, (2019) 3474.
[17] J. C. Santos-Ceballos, F. Salehnia, A. Romero, X. Vilanova, and E. Llobet: IEEE Sens. J., 24, (2024) 9366.
[18] S.-F. Tseng, P.-S. Chen, S.-H. Hsu, W.-T. Hsiao, and W.-J. Peng: Appl. Surf. Sci., 620, (2023) 156847.
[19] Z. Peng, L.-Q. Tao, S. Zou, C. Zhu, G. Wang, H. Sun, and T.-L. Ren: Chem. Eng. J., 428, (2022) 131079.
[20] L. Yang, G. Zheng, Y. Cao, C. Meng, Y. Li, H. Ji, X. Chen, G. Niu, J. Yan, Y. Xue, and H. Cheng: Microsyst. Nanoeng., 8, (2022) 78.
[21] L. Yang, N. Yi, J. Zhu, Z. Cheng, X. Yin, X. Zhang, H. Zhu, and H. Cheng: J. Mater. Chem. A., 8, (2020) 6487.
[22] M. Abdulhafez, G. N. Tomaraei, and M. Bedewy: ACS Appl. Nano Mater., 4, (2021) 2973.
[23] R. Murray, M. Burke, D. Iacopino, and A. J. Quinn: ACS Omega., 6, (2021) 16736.
[24] H. Wahab, V. Jain, A. S. Tyrrell, M. A. Seas, L. Kotthoff, and P. A. Johnson: Carbon., 167, (2020) 609.
[25] S. R. Kalidindi, M. Buzzy, B. L. Boyce, and R. Dingreville: Front. Mater., 9, (2022) 818535.
[26] H. Priyadarshi, G. Ahmed, D. Mishra, A. K. Srivastava, R. McGee, A. Shrivastava, and K. Singh: Crit. Rev. Solid State Mater. Sci., 1, (2024) 1.
[27] J. C. Santos-Ceballos, F. Salehnia, A. Romero, and X. Vilanova: Sci. Rep., 14, (2024) 10363.
[28] L. X. Duy, Z. Peng, Y. Li, J. Zhang, Y. Ji, and J. M. Tour: Carbon., 126, (2018) 472.
[29] Y. Zhang, S. Li, J. Zhang, Z. Pan, D. Min, X. Li, X. Song, and J. Liu: Sci. Rep, 3, (2013) 1
[30] Á. Peña, D. Matatagui, F. Ricciardella, L. Sacco, S. Vollebregt, D. Otero, J. López-Sánchez, P. Marín, and M. C. Horrillo: Appl. Surf. Sci., 610, (2023) 155393.
[31] D. H. Lee, and H. Yoo: Sensors 2022, 22, (2022) 9228.

(Received: June 4, 2024, Accepted: August 18, 2024)